STM Images of Subsurface Mn Atoms in GaAs: Evidence of Hybridization of Surface and Impurity States

J.-M. Jancu,[1] J.-Ch. Girard,[1] M. O. Nestoklon,[1,2] A. Lemaître,[1] F. Glas,[1] Z. Z. Wang,[1] and P. Voisin[1]

[1]*CNRS-Laboratoire de Photonique et de Nanostructures, route de Nozay, F-91460, Marcoussis, France*

[2]*Ioffe Physico-Technical Institute, Russian Academy of Sciences, 194021 St. Petersburg, Russia*

(Received 28 February 2008; published 4 November 2008)

We show that scanning tunneling microscopy (STM) images of subsurface Mn atoms in GaAs are formed by hybridization of the impurity state with intrinsic surface states. They cannot be interpreted in terms of bulk-impurity wave-function imaging. Atomic-resolution images obtained using a low-temperature apparatus are compared with advanced, parameter-free tight-binding simulations accounting for both the buckled (110) surface and vacuum electronic properties. Splitting of the acceptor state due to buckling is shown to play a prominent role.

DOI: 10.1103/PhysRevLett.101.196801 PACS numbers: 73.20.−r, 71.15.Ap, 73.61.Ey, 75.50.Pp

The development of scanning tunneling microscopy (STM) has expanded the applications of imaging to new areas of nanosciences and engineering such as atom or molecule identification, manipulation and nanostructuring [1–3]. Both spectroscopic and topological information is accessible, and quantum-size objects can be probed in real space with atomic resolution. In particular, there is growing interest in the STM images of quantum dots [4] and subsurface impurity states in semiconductors [5–8]. Although the well-accepted Tersoff and Hamann's theory [9] simply relates the tunneling current to the local density of states (LDOS) at the tip position, the interpretation of specific experiments on localized states is still a matter of debate: on the one hand, the interaction between the surface and the quantum object under investigation must be examined; on the other hand, particularly in the case of deep bound-states, the carrier escape toward the extended band states may play a role [7]. In the last few years, acceptors in GaAs have attracted much attention because the shape of the images revealed strong and unexpected chemical signatures: from triangles in the case of shallow acceptors like carbon [7] and zinc [6], to asymmetric butterfly for the deep acceptor manganese [5]. So far, theoretical work has concentrated mostly on comparison of STM images with cross sections of the bulk-impurity wave function [5]. In this Letter, we report on experimental data obtained with a low-temperature apparatus and compare these results with advanced tight-binding (TB) calculations. We first point that the STM image cannot reflect the LDOS of the impurity: indeed, empty-state STM images show only the group-III elements whereas the neutral acceptor wave function is distributed over the different chemical species. In fact, 65% of the bulk impurity LDOS is located around As sites that do not show up in empty-state STM images. Worse, the experimental images show inverted symmetry with respect to calculated bulk wave function. We prove that the image actually results from the hybridization between intrinsic surface states and the impurity state. Supercell calculations based on the $sp^3d^5s^*$ tight-binding model [10], including the buckled (110) surface as well as vacuum, are performed and reproduce nicely the experimental images. Splitting of the acceptor state due to intrinsic strain associated with buckling is shown to play a prominent role.

The sample used in this study was grown by molecular beam epitaxy on a GaAs (001) substrate at 420 °C. It consists of two 40 nm-thick GaAs layers doped with 2×10^{18} Mn cm^{-3}, embedded between 30 nm-thick GaAs conducting layers doped with 1×10^{19} Be cm^{-3}. The low temperature epitaxial growth was chosen in order to minimize the segregation of Mn atoms, and the codoping was needed because dilute Mn-doped GaAs is insulating below 77 K. The sample is cleaved *in situ* and exposes in a controlled manner the (110) or $(1\bar{1}0)$ surface. Figure 1(a) shows a mosaic of three overlapping constant-current topographical images measured at $T = 77$ K with sample-to-tip voltage $V_{st} = +1.7$ V and current $I_t = 100$ pA, and Fig. 1(b) an atomic-resolution image ($V_{st} = 1$ V, $I_t = 100$ pA) showing a few impurities. Note that for $V_{st} = 1$ V, there is no current injection into extended conduction band states. The atomic texture of Fig. 1(b) shows only a rectangular 5.65×4 Å^2 2 D lattice corresponding to a single species sublattice, while a (110) or $(1\bar{1}0)$ surface (see Fig. 2) exposes both Ga and As atoms. For *n*-doped GaAs, this feature was explained [11,12] in the 1990s: for positive V_{st}, electrons flow from the tip to empty surface states, consisting mostly of empty Ga dangling bonds, whereas for negative V_{st}, electrons flow from occupied surface states (mostly As dangling bonds) to the tip. This is why the image at positive V_{st} shows the rectangular sublattice formed by Ga surface atoms and not the characteristic zigzag chains of Ga and As atoms. The different shapes associated with Be (triangle) and Mn (butterfly) dopants are observed simultaneously in Fig. 1(a) and 1(b).

Clearly, the texture of image within an impurity is essentially identical to that in the background. Conversely, the

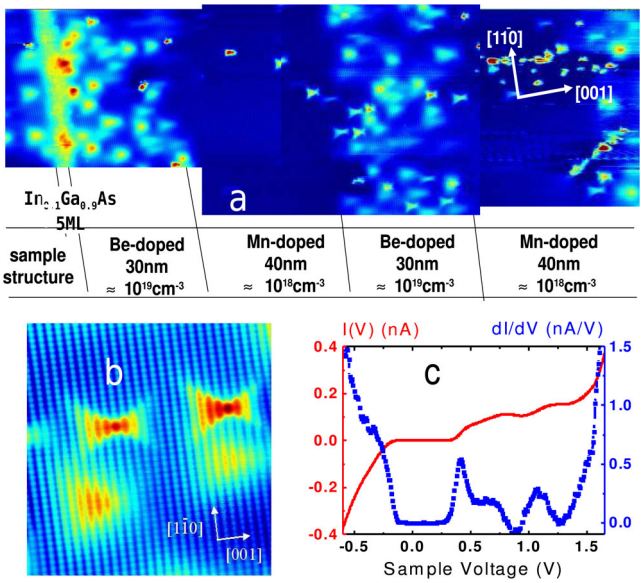

FIG. 1 (color online). (a) Mosaic of three overlapping topographical images measured at $T = 77$ K, on a (110) surface, with sample-to-tip voltage $V_{st} = +1.7$ V, current $I_t = 100$ pA. The Be-doped and Mn-doped GaAs layers are clearly identified. The triangular-shaped and butterflylike images correspond to Be and Mn dopants, respectively. (b) Atomic-resolution image ($V_{st} = 1$ V, $I_t = 100$ pA) showing a few impurity states. (c) Typical $I_t(V_{st})$ and dI_t/dV_{st} curves measured at fixed height in the center of a Mn impurity image.

LDOS of a neutral acceptor state in bulk GaAs must be spread over both types of atomic sites because it is built from zone center valence states that are known to have 70% As and 30% Ga character. This can be observed in the calculations of Ref. [5], and is further evidenced by the present $sp^3d^5s^*$ TB approach. Mn is a deep acceptor whose binding energy (113 meV) is governed by a strong central cell correction. In a TB frame, this local potential is associated with Mn d states and their hybridization with p states on neighboring As, a situation often handled perturbatively by shifting the on-site energy of a virtual group-III element [5] and changing the nearest-neighbor interactions. To go beyond this approximation, we constructed transferable Slater-Koster parameters using an empirical spd nearest-neighbor model with the nominal atomic structures: $4s^24p^14d^05s^0$ for Ga, $3d^54s^24p^0$ for Mn, and $4s^24p^34d^05s^0$ for As. The parameters were optimized to fulfill the requirement of agreement with *ab-initio* calculations, keeping nearly unchanged As one-site parameters between MnAs and GaAs for different crystal structures (hexagonal and cubic). Electronic band structure calculations are performed by considering a 4096-atom supercell of zinc-blende GaAs (45 Å × 45 Å × 45 Å) in which one Ga atom is replaced by Mn. Screened Coulomb interaction between the Mn ion and remote hole is included by shifting on-site energies accordingly. The atomic coordinates are relaxed using Keating's valence-force-field approach. A neutral acceptor A_0 bound state is found 90 meV above the valence-band edge, which is in fair agreement with experiment for the A_0 state of Mn [13]. The main limitation of the present calculations is the neglect of short-range p-d exchange interaction giving a magnetic contribution to the binding energy of 25 meV [14]. A 3D plot of the bound state LDOS and corresponding cross sections in the (110) and (1$\bar{1}$0) planes located 3 atomic planes away from the impurity center are shown in Fig. 2. The similar weights of Ga and As in the wave function are obvious (see also left column in Fig. 4). Note that the cross sections in (110) and (1$\bar{1}$0) planes obey the rotoinversion symmetry about the impurity center, which is also observed in our measured STM images. Strikingly, the cross section in the (110) plane shows a butterfly with a stronger right wing, while the STM image [see Fig. 1(b)] has a stronger left wing in the same plane, for the same orientation of the [001] axis. The theoretical result is astonishingly stable with respect to details of the modeling, and actually depends only on the binding energy. Noteworthily, the asymmetry is more pronounced than in previous calculations [5]. This is a direct consequence of the GaAs valence-band warping, much better reproduced in the $sp^3d^5s^*$ than in the sp^3 model [15].

The strong difference between textures of STM images and cross sections of a bulk impurity suggests that the former is actually formed by hybridization of the impurity and surface states. Providing that the interaction is weak enough for a perturbative approach to be valid, the wave function of this mixed state can be written as a linear combination $|\psi\rangle = \alpha|i\rangle + \int \rho(\boldsymbol{k})|s, \boldsymbol{k}\rangle d\boldsymbol{k}$ of the impurity wave function $|i\rangle$ and surface band wave functions $|s, \boldsymbol{k}\rangle$, where $\boldsymbol{k}$ is the two-dimensional wave vector. There is implicit summation over different types of surface states. The amplitude of surface band admixture is expressed to first order as $\rho(\boldsymbol{k})/\alpha = [\frac{V(\boldsymbol{k})}{E_i - E_s(\boldsymbol{k})} - I(\boldsymbol{k})]$, where E_i is the

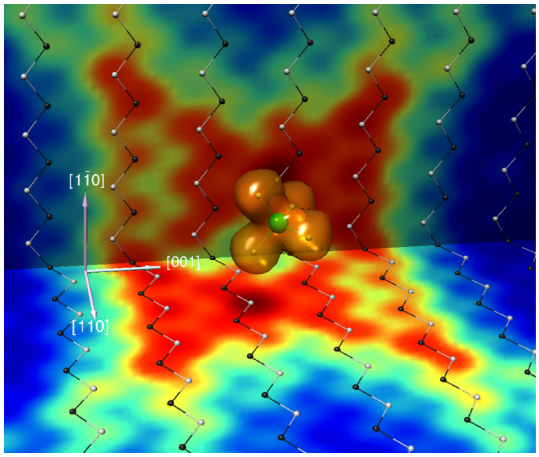

FIG. 2 (color online). 3D plot of the impurity bound state, and cross sections (Log scale) in the (110) and (1$\bar{1}$0) planes situated 3 atomic planes apart from the impurity center. Atomic positions in the section planes are shown as black (Ga) and white (As) circles.

impurity state energy and $E_s(\boldsymbol{k})$ the surface band dispersion. $I(\boldsymbol{k}) = \langle s, \boldsymbol{k}|i\rangle$ and $V(\boldsymbol{k}) = \langle s, \boldsymbol{k}|U_i|i\rangle$ [where $U_i(\boldsymbol{r})$ is the impurity potential] are the overlap and perturbation integrals, respectively. While $I(\boldsymbol{k})$ should be small compared to unity, the evaluation of $V(\boldsymbol{k})$ requires precise knowledge of the impurity potential and detailed description of the surface band structure. This analysis provides insight into the mechanism of mixing between surface bands and impurity level, but cannot bring quantitative information. The latter is obtained by simulating the physical situation numerically. We first prove that the present TB approach accounts fairly well for the surface states by calculating the electronic properties of a superlattice where 40 monolayers of GaAs alternate with 3 nm of vacuum. Here vacuum is described in terms of a zinc blende crystal with TB parameters reproducing the dispersion of the free electron, and having a dielectric constant equal to unity. As discussed in Ref. [10], the $sp^3d^5s^*$ model is close enough to numerical completion to allow for such folding of the free electron band structure. The rearrangement of near-surface atoms known as buckling relaxation, which prevents the formation of surface states inside the gap [12,16], is taken into account in the calculation. The band structure and LDOS of buckled GaAs(110) surface are found in excellent agreement with *ab initio* results, as evidenced in Fig. 3 for the first empty dangling-bond state C3 [12,16]. The calculation closely reproduces the general properties of C3 obtained from *ab initio* modeling in terms of energy, the strong Ga contribution to the surface wave function, and attenuation within the crystal and vacuum. The slow decay of surface states inside the crystal certainly plays a major role in their strong interaction with subsurface localized states. Next, a Mn dopant is added in the GaAs slab, in the nth plane below the surface. In Fig. 4, the simulated STM (SSTM) images formed by the cross sections of the corresponding states in the first plane of "vacuum atoms" (i.e., 2 Å above the surface [17]) are compared with bulk-impurity cross sections (BICS) and with the experimental results for $n = 3$ to $n = 5$. For these depths, the calculated acceptor binding energy shows little change (from 90 to 85 meV). All the images exhibit a $(1\bar{1}0)$ mirror plane, but for even n, this plane goes through a row of surface Ga atoms while for odd n, it goes through a row of surface As atoms. Major differences between the two types of theoretical images are clearly observed. The most obvious one is the orientation of the butterfly showing a stronger left wing in SSTM and experimental images instead of a stronger right wing in BICS. This symmetry reversal is due to intrinsic strain associated with the buckling relaxation. We find that this surface-induced strain breaks the fourfold degeneracy of the bulk-impurity state [18] in two twofold states separated by an amount of about 50 meV, so that only the ground A_0 state is occupied by a hole, even in room temperature experiments. While the LDOS integrated over the two states gives an image similar to the BICS, the ground state alone shows the opposite symmetry. The fact that buckling affects not only the surface layer but actually extends down to the 4th sublayer [16] plays an important role in the splitting value, a large fraction of the hole wave function experiencing the strained volume. This effect would dominate the *p-d* exchange, explaining the remarkable similarity of GaAs:Mn and GaP:Cd STM images [19]. The other striking difference concerns the respective weights of anion and cation sites. To be specific, we focus the discussion on the case of $n = 4$. BICS in that case is centered on a row of Ga atoms, and one easily checks that most of the bright spots correspond to As sites

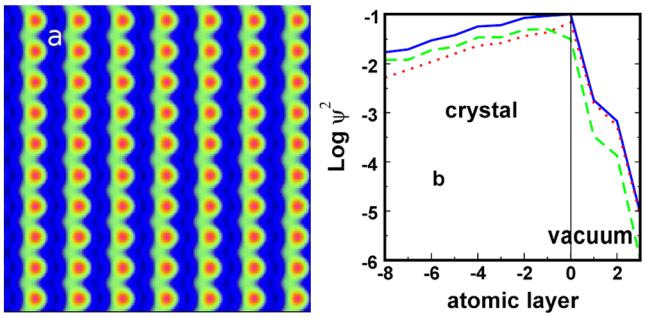

FIG. 3 (color online). (a) Log-scale LDOS plot of the surface state C3, at 0.5 eV above the conduction band minimum. LDOS is calculated at 2 Å above the (110) surface. (b) Decays of C3 in crystal and vacuum along the [110] direction (solid line) and site-projected anion (dashed line) and cation (dotted line) contributions.

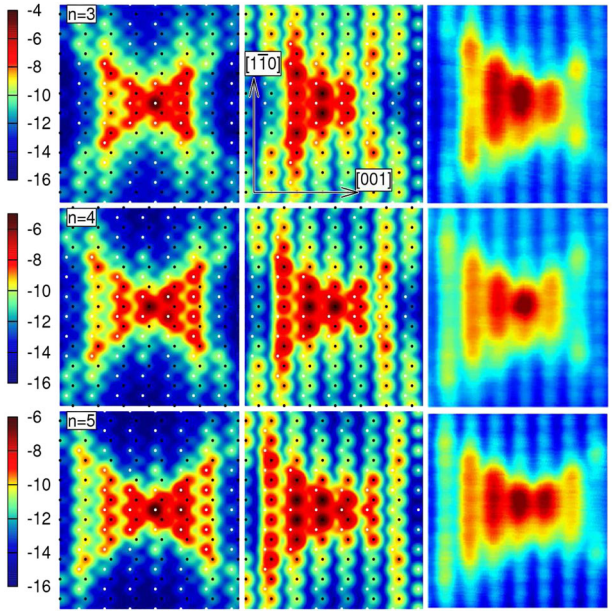

FIG. 4 (color online). Bulk impurity cross section (BICS) (left), simulated STM images (SSTM) (center), and experimental STM images (right) of a Mn neutral acceptor located n monolayers ($n = 3$ to 5) below the (110) surface. BICS is calculated in a (110) plane, n atomic planes away from the impurity, and SSTM 2 Å above the surface. SSTM LDOS is multiplied by 10^4 with respect to BICS. As (white) and Ga (black) positions on the surface are indicated.

(64% of LDOS). More precisely, the As sites dominate strongly the right part of the image, while Ga and As have similar weights in the left part. Conversely, in the SSTM image, the Ga sites clearly dominate (70% of LDOS) and As show up only near the center of the image. Similar conclusions are drawn for the $n = 3$ and $n = 5$ cases, with the difference that corresponding images appear centered on a row of As sites. These features illustrate that hybridization strongly filters out the As component from BICS. This finding is by no way trivial: building on the perturbative model, one might have expected that the impurity state interacts preferentially with energetically closer valence-type surface states that have a strong As component in vacuum [12]. The overall agreement between SSTM and experimental images allows a precise identification of the impurity depth [20].

We finally comment spectroscopic data on these images. $I_t(V_{st})$ curves at fixed height were recorded on many Mn images, and a typical spectrum is shown in Fig. 1(c). These curves show a threshold whose position varies between 100 and 600 mV. A clear correlation between threshold voltage and distance to the heavily p-doped layer is observed, suggesting that variations of the tip-induced band bending is the main cause of threshold variation. Images of a given impurity show little dependence on V_{st} until V_{st} exceeds 1.5 V and I_t starts integrating contributions from tunneling to conduction band states. We point that STM measures basically a dc current, that can flow only if the tunneling electron escapes out of the bound state at a rate faster than the injection rate. Since when changing V_{st}, one changes the impurity environment from hole depletion to hole accumulation [8], the very mechanism of electron escape probably changes whereas the image is not affected. This suggests that the voltage threshold merely corresponds to a condition for the impurity to be effectively in an A_0 state, or for the electron to escape fast enough. As pointed in Ref. [7], the detailed mechanism of electron escape towards extended band states in STM spectroscopy certainly deserves more attention but in the present case it does not seem to influence the image itself.

In conclusion, we have shown that STM images of subsurface impurities are formed due to splitting of impurity state and hybridization with intrinsic surface states. These features are general and apply to other types of near-surface localized states like images of shallow impurities [such as Be in Fig. 1(b)] and quantum dots. Realistic tight-binding calculations including the surface allow comparison with experiment at an unprecedented level of precision. The method can be extended to many different nanometer-sized objects, up to a present limit of a few million atom supercells. Our analysis reveals that the impurity state acts as an inner experimental probe of surface states and their extension in the crystal.

The authors thank Drs. J-Ch. Harmand and L. Largeau for valuable discussions, Ch. David and Ch. Dupuis for technical assistance. Calculations were performed at the IDRIS-CNRS supercomputing center (project CAPnano). J. M. J. is supported by the ''SANDIE'' NoE of the EC and M. N. by RFBR and Dynasty Foundation.

[1] S. W. Hla, L. Bartels, G. Meyer, and K. H. Rieder, Phys. Rev. Lett. **85**, 2777 (2000).
[2] K. F. Braun and K. H. Rieder, Phys. Rev. Lett. **88**, 096801 (2002).
[3] D. Kitchen, A. Richardella, J.-M. Tang, M. E. Flatté, and A. Yazdani, Nature (London) **442**, 436 (2006).
[4] J. Marquez, L. Geelhaar, and K. Jacobi, Appl. Phys. Lett. **78**, 2309 (2001).
[5] A. M. Yakunin, A. Yu. Silov, P. M. Koenraad, J. H. Wolter, W. Van Roy, J. De Boeck, J.-M. Tang, and M. E. Flatté, Phys. Rev. Lett. **92**, 216806 (2004).
[6] G. Mahieu, B. Grandidier, D. Deresmes, J. P. Nys, D. Stievenard, and Ph. Ebert, Phys. Rev. Lett. **94**, 026407 (2005).
[7] S. Loth, M. Wenderoth, L. Winking, R. G. Ulbrich, S. Malzer, and G. H. Dohler, Phys. Rev. Lett. **96**, 066403 (2006).
[8] F. Marczinowski, J. Wiebe, J.-M. Tang, M. E. Flatté, F. Meier, M. Morgenstern, and R. Wiesendanger, Phys. Rev. Lett. **99**, 157202 (2007).
[9] J. Tersoff and D. R. Hamann, Phys. Rev. Lett. **50**, 1998 (1983); Phys. Rev. B **31**, 805 (1985).
[10] J.-M. Jancu, R. Scholz, F. Beltram, and F. Bassani, Phys. Rev. B **57**, 6493 (1998).
[11] R. M. Feenstra, Joseph A. Stroscio, J. Tersoff, and A. P. Fein, Phys. Rev. Lett. **58**, 1192 (1987).
[12] Ph. Ebert, B. Engels, P. Richard, K. Schroeder, S. Blugel, C. Domke, M. Heinrich, and K. Urban, Phys. Rev. Lett. **77**, 2997 (1996).
[13] R. A. Chapman and W. G. Hutchinson, Phys. Rev. Lett. **18**, 443 (1967).
[14] A. K. Bhattacharjee and C. Benoit a la Guillaume, Solid State Commun. **113**, 17 (1999).
[15] T. B. Boykin, G. Klimeck, and F. Oyafuso, Phys. Rev. B **69**, 115201 (2004).
[16] B. Engels, P. Richard, K. Schroeder, S. Blugel, Ph. Ebert, and K. Urban, Phys. Rev. B **58**, 7799 (1998).
[17] experimental conditions rather correspond to a tip to surface distance of 4 Å, but due to the fast decay of surface states in the vacuum, we reach numerical underflow and loose image resolution at this distance. Note that images of state C3 at 2 Å and 4 Å are quite similar.
[18] The STM image can actually be distorded when straining the impurity environment, see A. M. Yakunin *et al.*, Nature Mater. **6**, 512 (2007).
[19] C. Çelebi, P. M. Koenraad, A. Yu. Silov, W. Van Roy, A. M. Monakhov, J.-M. Tang, and M. E. Flatté, Phys. Rev. B **77**, 075328 (2008).
[20] J. K. Garleff, C. Çelebi, W. Van Roy, J.-M. Tang, M. E. Flatté, and P. M. Koenraad, Phys. Rev. B **78**, 075313 (2008).